Investigation of induced fission of ^{nat}Pb by accelerated ^{7}Li ions

N. A. Demekhina*
Yerevan Physics Institute, Alikhanyan Brothers 2, Yerevan 0036, Armenia
Joint Institute for Nuclear Research (JINR), Flerov Laboratory of Nuclear Reactions (LNR), Joliot-Curie 6, Dubna 141980, Moscow region Russia

G. S. Karapetyan†
Instituto de Fisica, Universidade de São Paulo, P. O. Box 66318, 05389-970 São Paulo, SP, Brazil

V. Guimarães‡
Instituto de Fisica, Universidade de Sao Paulo, P. O. Box 66318, 05389-970 S ao Paulo, SP, Brazil

The cross-section of the ^{nat}Pb binary fission, induced by ^{7}Li ions at 245 MeV energy, was measured and the fission product cross-sections studied by means of activation analysis in the off-line regimen. The analysis of charge and mass distributions of fission products allows to calculate the fission cross-section. The recoil technique ("thick target- thick catcher"), based on the two step model mathematical formalism, is used for the determination of the kinematical characteristics of reaction products. The data concerning transferred linear momentum provides information on the initial projectile-target interaction, and is compared to measurements of the proton-induced fission.

PACS numbers: 25.85.Ge, 24.75.+i, 25.85.-w

I. INTRODUCTION

The investigation of the mechanism of nucleon-nucleus and nucleus-nucleus collisions at low and intermediate energies is a source of understanding the interplay between macroscopic and microscopic aspects of interaction in hot, high-spin nuclear matter. The way how the collective nature of the nuclear fission is modified, according to the incident projectile type, the transferred energy, and the momentum as well, is a question of interest to both experimentalists and theorists. A considerable amount of measurements were performed for nucleon-induced fission on the different heavy nuclei [1]. Notwithstanding, a survey on the literature displays that there is a considerable lack of experimental data for the heavy-ion-induced fission. They are mainly presented by some works with carbon projectile [2, 3], α-particles [4]. The first and single comprehensive investigation on ^{208}Pb target by ^{6}Li-ion beam in the energy range of 74.8-94.4 MeV was accomplished in [5]. The authors above mentioned quantitatively studied the decay properties of heavy nuclei, at high angular momentum and high excitation energy. It is of particular interest to investigate how to change the fission cross-section with angular momentum transferred in the entrance channel of the reaction for nucleon- and heavy-ion-induced fission. According to the classical rotating-liquid-drop model (RLDM) [6] and various other theoretical presentations [7-10], the fission barrier height should decrease monotonically, and eventually vanishes as the transferred angular momentum increases.

In this paper we present the new results regarding the measurements about a lead target in ^{7}Li-induced fission reaction at 245 MeV. The fission fragments charge and mass distributions are used to determine the fission cross section. Based on the dynamic model [8] it is possible to extract the angular momentum imparted to the fissioning nucleus at the interaction initial stage. It is further compared to the obtained experimental data. Furthermore, a small part of the experimental data cross-sections presented in [11] is recalculated, due to some systematic uncertainties concerning the fission fragment registration efficiency.

II. EXPERIMENTAL PROCEDURE

A pure lead target, having a natural isotopic composition (^{nat}Pb: 1.48% ^{204}Pb, 23.6% ^{206}Pb, 22.6% ^{207}Pb, and 52.3% ^{208}Pb), was prepared in the form of an assembly of seven lead foils 12 μm thick. The target was exposed

*Electronic address: demekhina@nrmail.jinr.ru
†Electronic address: ayvgay@ysu.am
‡Electronic address: valdirg@dfn.if.usp.br

to an accelerated ^{7}Li-ion beam of energy 35 MeV/u from the U-400M cyclotron in the Joint Institute for Nuclear Research (JINR), Dubna, Russia. The irradiation time was 40 min at ion beam intensity of about 10^{10} nuclei per second. Aluminum foils 20 μm thick were used to collect the recoil nuclei on the two sides of the target in forward and backward directions relatively beam, which allow to provide the solid angle about 2π. The catcher foils thickness was larger than the longest recoil range. The fission fragment cross-sections were measured in the off-line mode by using the induced-activity method. The ranges and ratio of forward and backward emitted radioactive reaction products were recorded also. The measurements of the spectra of γ-rays emitted in the decays of radioactive fission products had started 10 min after the completion of the irradiation and lasted five months by using HpGe detector with energy resolution 0.23% at an energy of 1332 keV. The energy-dependent detection efficiency of the HpGe detector was measured with standard calibration sources of ^{22}Na, ^{54}Mn, $^{57;60}$Co, ^{137}Cs, ^{154}Eu, ^{152}Eu, and ^{133}Ba. The half-lives of identified isotopes were within the range between 15min and 1 yr. The error in determining cross sections depended on the following factors: the statistical significance of experimental results ($\leq$ 2-3%), the accuracy in measuring the target thickness and the accuracy of tabular data on nuclear constants ($\leq$ 3%), and the errors in determining the detector efficiency with allowance for the accuracy in calculating its energy dependence ($\leq$ 10%). Nuclear properties, used for identification of observed isotopes as nuclear transition energies, intensities, and half-lives were taken from literature [12].

The reaction fragment production cross-sections in the absence of a parent isotope — that may give a contribution in measured cross-section via $\beta^{\pm}$- decays — are usually considered as an independent yield (I) and determined by using the following equation:

$$\sigma = \frac{\Delta N\, \lambda}{N_p\, N_n\, k\, \epsilon\, \eta\, (1 - \exp(-\lambda t_1)) \exp(-\lambda t_2)(1 - \exp(-\lambda t_3))} \tag{1}$$

where σ is the cross-section of the reaction fragment production (mb); ΔN is the area under the photopeak; N_p is the proton beam intensity (min^{-1}); N_n is the number of target nuclei (in 1/cm^2 units); t_1 is the irradiation time; t_2 is the time of exposure between the end of the irradiation and the beginning of the measurement; t_3 is the time measurement; λ is the decay constant (min^{-1}); η is the intensity of γ-transitions; k is the total coefficient of γ-ray absorption in target and detector materials, and ϵ is the γ-ray-detection efficiency.

In the case where the yield of a given isotope includes a contribution from the $\beta^{\pm}$-decay of neighboring unstable isobars, the cross section calculation becomes more complicated [13]. If the formation probability for the parent isotope is known from experimental data, or if it can be estimated on the basis of other sources, hence the independent yields of daughter nuclei can be calculated by the relation:

$$\sigma_B = \frac{\lambda_B}{(1 - \exp(-\lambda_B t_1))\, \exp(-\lambda_B t_2)(1 - \exp(-\lambda_B t_3))} \times$$
$$\left[\frac{(\Delta N)_{AB}}{N_\gamma\, N_n\, k\, \epsilon\, \eta} - \sigma_A\, f_{AB}\, \frac{\lambda_A\, \lambda_B}{\lambda_B - \lambda_A} \left(\frac{(1 - \exp(-\lambda_A t_1))\, \exp(-\lambda_A t_2)\, (1 - \exp(-\lambda_A t_3))}{} \lambda_A^2 \right.\right.$$
$$\left.\left. - \frac{(1 - \exp(-\lambda_B t_1))\, \exp(-\lambda_B t_2)\, (1 - \exp(-\lambda_B t_3))}{} \lambda_B^2 \right) \right], \tag{2}$$

where the subscripts A and B label variables referring to, respectively, the parent and the daughter nucleus; the coefficient f_{AB} specifies the fraction of A nuclei decaying to a B nucleus (f_{AB} =1, when the contribution from the β-decay corresponds 100%); and $(\Delta N)_{AB}$ is the total photopeak area associated with the decays of the daughter and parent isotopes. The effect of the precursor can be negligible in some limiting cases: where the half-life of the parent nucleus is very long, or in the case where its contribution is very small. In the case when parent and daughter isotopes could not be separated experimentally, the calculated cross-sections are classified as cumulative ones (C). It should be mentioned that using of induced-activity method imposes several restrictions on the registration of the reaction products. For example, it is not possible to measure a stable and short-lived isotopes.

III. EXPERIMENTAL DATA ANALYSIS

The experimental cross-sections of fission fragment production in the mass range of $61 \leq A \leq 147$ amu are presented in Table 1and Fig. 1. In order to obtain a complete picture of the charge and mass distributions of fission products, it is necessary to estimate the cross-sections of isotopes unmeasurable by the induced-activity method. In the present

work, therefore, the analysis of the charge distribution was performed by assuming the following Gaussian function for charge distribution [13]:

$$\sigma_{A,Z} = \frac{\sigma_A}{(C\pi)^{1/2}} \exp\left(-\frac{(Z - Z_p)^2}{C}\right), \tag{3}$$

where $\sigma_{A,Z}$ is the independent cross-section for a given nuclide production with atomic charge Z and a mass number A; σ_A is the total isobaric cross-section of the mass chain A, Z_p denotes the most probable charge for a given isobar, and C denotes the width parameter of the charge distribution.

Table 1. Cross-sections of fission fragments

Element	Type	σ, mb	Element	Type	σ, mb
^{61}Cu	C	$\leq$0.11	^{99}Mo	C	10.72 $\pm$1.08
^{62}Zn	C	$\leq$0.04	^{99m}Tc	I	0.26$\pm$0.03
^{65}Ni	I	$\leq$0.20	^{101m}Rh	I	0.78 $\pm$0.08
^{65}Zn	I	0.40$\pm$0.08	^{102m}Rh	I	0.42$\pm$0.03
^{65}Ga	C	$\leq$0.02	^{103}Ru	C	15.65 $\pm$1.51
^{66}Ni	I	0.11$\pm$0.02	$^{105(m+g)}$Rh	I	13.74$\pm$1.37
^{66}Ga	I	$\leq$0.035	^{106}Ru	C	11.11$\pm$1.11
^{67}Cu	C	0.72$\pm$0.07	^{106m}Rh	C	7.60$\pm$0.91
^{67}Ga	C	0.026$\pm$0.003	^{110m}Ag	I	2.70$\pm$0.40
^{69}Ge	C	$\leq$0.45	$^{111(m+g}$)Ag	C	10.18$\pm$1.02
^{71m}Zn	I	0.96$\pm$0.14	^{111}Cd	I	$\leq$0.63
^{72}Zn	I	$\leq$0.02	^{112}Pd	C	3.10 $\pm$0.31
^{72}Ga	I	0.25$\pm$0.02	^{112}Ag	I	2.10$\pm$0.25
^{73}Ga	I	0.63$\pm$0.08	$^{113(m+g)}$Ag	C	2.45$\pm$0.37
^{74}As	I	0.37$\pm$0.04	$^{113(m+g)}$Sn	C	3.34$\pm$0.50
^{75}Se	I	0.19$\pm$0.01	^{115}Cd	C	1.25$\pm$0.13
^{75}Br	C	$\leq$0.017	^{117g}Cd	C	1.26 $\pm$0.13
^{76}As	I	2.77$\pm$0.28	^{117m}Cd	C	1.31$\pm$0.16
$^{77(m+g)}$Ge	C	2.00$\pm$0.20	^{117m}Sn	I	2.83$\pm$0.28
$^{77(m+g)}$Br	I	$\leq$0.02	$^{118(m+g)}$Sb	I	1.90$\pm$0.20
^{78}Ge	I	2.40$\pm$0.24	^{120m}Sb	I	3.80$\pm$0.40
^{78}As	C	$\leq$1.98	^{121g}Te	I	4.60$\pm$0.69
^{81m}Se	C	$\leq$0.77	^{121m}Te	I	1.95$\pm$0.29
$^{82(m+g}$)Br	I	1.67$\pm$0.17	^{121}I	I	$\leq$0.45
^{83}Rb	C	1.85$\pm$0.19	$^{122(m+g)}$Sb	I	2.74$\pm$0.30
^{84}Br	C	4.80$\pm$0.50	^{123m}Te	I	4.73$\pm$0.50
$^{84(m+g)}$Rb	I	1.14$\pm$0.11	^{123}I	I	0.94$\pm$0.10
^{85g}Sr	I	1.80 $\pm$0.18	^{123}Xe	C	$\leq$0.04
^{85m}Sr	I	$\leq$0.34	$^{124(m+g)}$Sb	I	2.60$\pm$0.26
^{85g}Y	C	0.35 $\pm$0.04	^{124}I	I	1.25$\pm$0.13
$^{86(m+g)}$Rb	I	7.04$\pm$1.05	^{125}Sb	C	0.86$\pm$0.09
^{87g}Y	I	0.68$\pm$0.07	^{126}I	I	1.82$\pm$0.19
^{87m}Y	C	0.50$\pm$0.06	^{127}Sb	C	$\leq$0.06
^{88}Y	C	1.12$\pm$0.35	$^{127(m+g)}$Xe	I	0.29$\pm$0.03
^{89}Rb	C	2.20$\pm$0.22	^{128}Sb	C	0.38$\pm$0.04
$^{89(m+g)}$Zr	C	0.48$\pm$0.05	^{129}Sb	C	$\leq$0.55
^{90m}Y	I	3.80$\pm$0.40	^{129m}Te	I	1.62$\pm$0.17
^{91}Sr	C	4.94 $\pm$0.50	^{129g}Ba	C	$\leq$0.73
^{91m}Y	I	$\leq$0.32	^{129m}Ba	C	$\leq$0.19
^{92}Sr	C	5.80 $\pm$0.58	$^{130(m+g)}$I	I	0.29$\pm$0.03
^{92}Y	I	2.00 $\pm$0.20	^{131m}Te	C	$\leq$0.50
^{93}Y	C	13.00$\pm$1.30	^{132}Te	C	$\leq$0.02
^{94}Y	C	8.90$\pm$0.90	^{132}Cs	I	0.37$\pm$0.04
^{95}Zr	C	12.00 $\pm$1.20	$^{133(m+g)}$I	C	$\leq$1.00

Element	Type	σ, mb	Element	Type	σ, mb
$^{95(g+m)}$Nb	I	9.84±1.00	^{133m}Ba	I	0.30±0.06
^{95g}Tc	I	≤0.10	^{139}Ba	C	≤0.45
$^{96(g+m)}$Tc	I	≤0.03	$^{139(m+g)}$Ce	C	1.17±0.12
^{97}Zr	C	3.12±0.31	^{140}Ba	C	0.33±0.03
$^{97(g+m)}$Nb	I	3.55±0.36	^{140}La	I	0.18±0.02
^{97}Ru	C	≤0.20	^{141}La	I	≤0.30
^{98m}Nb	I	1.50±0.16	^{147}Gd	C	≤0.03

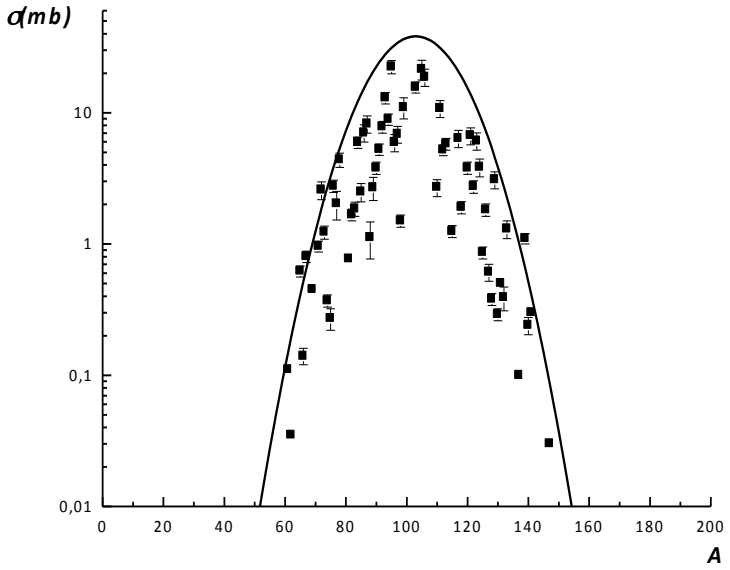

Fig. 1. Fission-product mass yields from 245 MeV ^{7}Li-induced fission on ^{nat}Pb: the total fission cross-section (thick black continuous curve), experimental data (■) fission of compound uncle.

As it was reported earlier in the experiments for fission analysis with different projectile at low energies on heavy targets ($209 \leq A \leq 238$) [14-16] the charge distribution widths are practically independent on the excitation energy and projectile and target nuclear properties. The assumption of the constant width parameter for different mass chains ($C = 1$) was used in the fitting procedure, by using least-squares method for obtaining Z_p and σ_A parameters. In the fitting process, at first, independent yields are used. Hence, during successive approximation procedures, the estimation of the independent component of cumulative cross-section are extracted. The evaluated most probable charges (Z_p) are summarized in Table 2. The values obtained are in good agreement with data on the fission of Bi target by ^{12}C [15].

Table 2. Values of the most probable charge Z_p.

A	Z_p	σ_A	A	Z_p	σ_A
76	33±0.66	4.0±0.40	110	45.7±0.69	30.0±0.76
77	32.5±0.53	4.0±0.32	111	46.3±0.61	30.0±1.90
78	32.4±0.34	5.38±0.88	112	45.6±0.53	27.0±1.45
82	34.0±0.15	9.62±0.78	113	48.6±0.48	32.0±0.87
83	35.9±0.22	11.0±0.50	115	49.4±0.67	24.0±0.90
84	35.6±0.30	12.0±0.62	117	49.2±0.55	20.0±1.34
85	36.65±0.46	14.0±0.71	118	49.7±0.48	18.8±0.60
86	36.5±0.53	15.5±0.53	120	50.1±0.34	15.0±0.90
89	37.3±0.50	21.0±1.40	121	51.5±0.60	15.0±0.80
90	37.8±0.50	24.0±0.53	121	51.5±0.48	15.0±0.79
91	37.0±0.34	24.0±1.23	122	52.0±0.33	12.0±0.87
92	37.55±0.43	28.0±1.03	123	51.8±0.41	9.0±0.10
93	39.35±0.41	27.0±1.20	124	51.8±0.45	9.0±0.32
94	39.53±0.50	30.0±0.96	125	52.3±0.39	8.0±0.42
95	40.4±0.34	25.0±1.30	126	52.3±0.33	6.0±0.09
96	40.1±0.24	23.0±0.77	127	52.6±0.35	6.0±0.40
97	41.3±0.57	30.0±1.11	128	52.65±0.46	4.5±0.33
99	41.4±0.39	34.0±0.82	129	52.4±0.27	5.0±0.11
101	43.2±0.34	38.0±1.12	130	54.4±0.34	3.85±0.12
102	43.1±0.45	37.0±0.68	132	54.0±0.42	2.0±0.06
103	43.5±0.36	38.0±0.73	140	56.2±0.22	0.6±0.04
105	44.7±0.46	30.0±0.56	141	56.2±0.53	0.4±0.04
106	44.3±0.42	30.0±1.12			

Figure 2 (a, b, c) shows the calculated fractional cross-sections (cross-section of fragment production to total cross-section for given mass number), as well as their Gaussian charge distribution, for different isobaric chains, as a function of the difference $(Z_p - Z)$. It can be proposed that charge distributions of fission fragments are mainly determined by the properties of forming nuclei.

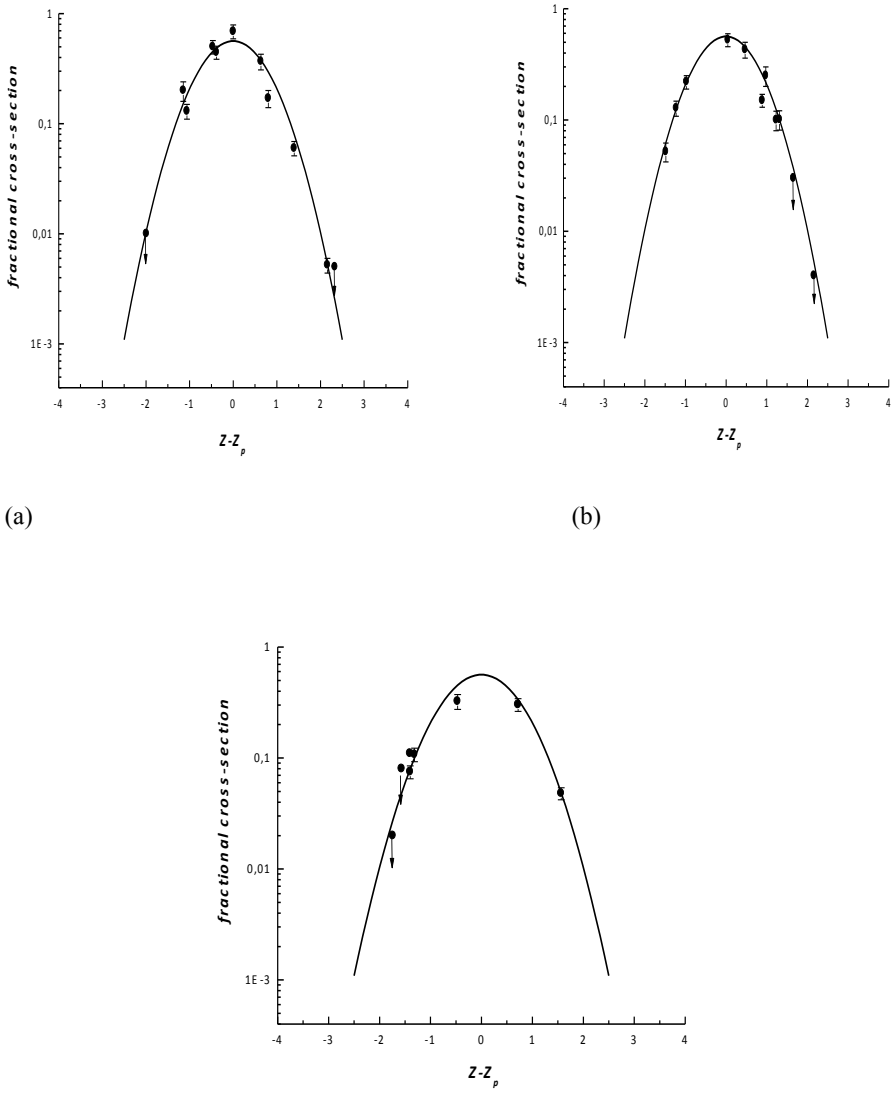

Fig. 2. The charge distributions of fission products in the 245 MeV ^{7}Li–induced fission of ^{nat}Pb for isobaric chains in the mass regions: (a)=72-78; (b)=115-118; (c)=125-130; experimental data (■). The curves are the estimated Gaussian distribution.

The mass distribution of fission fragments, constructed by using of obtained values of σ_A, is obtained by the fitting procedure. An assumption of the symmetric mass distribution in the Gaussian form [17] can used for that:

$$\sigma_f = \lambda_A \exp\left(-\frac{(A - M_A)^2}{\Gamma_A}\right) \tag{4}$$

The curve in eq. (4), representing the mass distribution, is defined by a height λ_A, a mean mass M_A, and a width Γ_A. The result of the summation over all mass numbers of the fission fragments allows the estimation of the fission cross-section. We multiple it by a factor 0.5, due to the two fission fragments in each event. In Fig. 1 the mass yield distribution, obtained by the fitting procedure, is represented by the solid curve. The values of the fit parameters, together with the fission cross-section, are tabulated in Table 3. The maximum of the mass distribution is arranged around $A = 103$. Therefore the average mass of the fissioning nucleus about 206 amu can be expected. In consequence of this result, the ∼9 nucleons (presumably neutrons) were emitted during fission process, in average. The nucleus-nucleus interaction in the entrance channel at energies 10 - 70 MeV/u should be changed as it is pointed in [18]. In this intermediate energy region, the complete fusion process at low limits are replaced partially by other processes, as the energy increases. Approximately 40% of the fission channel at this energy can result from complete fusion, as considered in [18] . Another part of the first stage of interaction is connected, perhaps, to incomplete fusion, or a significant pre-equilibrium contribution of the emission of nucleons or light nuclei.

Table. 3. Fitted values of the parameters in (4) and fission cross-section σ_f.

Γ_A	17.84±0.89
λ_A	38.25±2.3
M_A	102.98±0.2
σ_f (mb)	604.74±90.71

The measurements regarding recoil nuclei were analyzed in the frame of the two step vector model [19], described in detail in [11]. Considering these data, the relative amount of radioactive products in the forward (F) and backward (B) catch foils can be presented in the following form:

$$F = \frac{S_F}{S_F + S_B + S_T}, \qquad B = \frac{S_B}{S_F + S_B + S_T}, \tag{5}$$

where S_F , S_B, and S_T are the photopeak areas associated with the products under study in the catch foils and in the target. The results were used to calculate the forward-backward (F/B) ratio of product emission and the recoil ranges in the target material $R = 2W(F + B)$, where W is the thickness of the target in mg/cm^2.

From the range values, the associated kinetic energy T can be calculated. In the present work the Northcliffe-Schilling tables [20] are used directly to define T from the range values. In order to transform the ranges into the kinetic energy of fission fragments, the relation

$$R = KT^{N/2} \tag{6}$$

was regarded [19], where the parameters K and N are obtained for given Z and A, by fitting the range dependence on energy of accelerated ions. The mean excitation energy of the intermediate nucleus can be estimated by using the relation given in [21]:

$$\frac{E^*}{E_{CN}} = 0.8\frac{p_{\|}}{p_{CN}} \tag{7}$$

The recoil parameters calculated in present work are given in Table 4.

Table 4. Kinematical features of fission fragments.

Nucleus	F/B	$2W(F+B)$, mg/cm^2	T, MeV	E^*, MeV	$p_{\parallel}/p_{CN}$
^{72}Zn	1.11±0.22	13.22±2.64	107.41±21.48	68.68±11.64	0.33±0.06
$^{77(m+g)}$Br	1.16±0.14	13.36±1.60	100.17±12.02	82.32±11.52	0.42±0.06
$^{82(m+g)}$Br	1.17±0.14	11.79±1.41	96.25±11.55	84.28±11.79	0.43±0.06
^{83}Rb	1.17±0.08	10.25±0.72	93.15±6.52	80.36±7.88	0.41±0.04
$^{84(m+g)}$Rb	1.14±0.10	8.17±0.74	89.56±8.06	68.60±7.82	0.35±0.04
$^{87(m+g)}$Y	1.19±0.06	10.50±0.53	87.57±4.38	86.24±4.31	0.44±0.02
^{91}Sr	1.18±0.10	10.10±0.81	79.05±5.59	76.44±7.64	0.39±0.04
^{95}Zr	1.19±0.16	11.41±1.74	76.54±11.51	78.40±11.76	0.40±0.06
$^{95(g+m)}$Nb	1.23±0.11	11.36±1.02	77.22±6.56	90.16±7.84	0.46±0.04
$^{96(g+m)}$Tc	1.29±0.14	10.09±1.10	74.76±8.22	99.47±9.95	0.58±0.06
^{99}Mo	1.22±0.06	10.33±0.52	71.86±3.59	84.28±4.21	0.43±0.02
$^{105(m+g)}$Rh	1.17±0.09	10.07±0.81	70.95±5.65	66.64±3.99	0.34±0.02
$^{111(m+g)}$Ag	1.22±0.12	8.32±0.83	65.69±6.57	76.44±7.64	0.39±0.04
^{115}Cd	1.19±0.12	10.77±1.07	59.03±5.90	64.68±7.76	0.33±0.04
^{117m}Sn	1.43±0.17	7.69±0.92	53.50±6.42	119.56±15.54	0.61±0.08
^{120m}Sb	1.45±0.06	4.29±0.17	50.87±2.03	119.56±7.89	0.61±0.04
^{124}I	1.65±0.18	7.95±0.87	46.47±5.11	150.92±15.09	0.77±0.08

IV. 4 DISCUSSION

The total kinetic energy released in the fission process can be determined as a sum of the energies of two presumed fragments, consisting of 141.5±12.7 MeV, on average. This value is in fairly good agreement with the estimate 142.67 MeV, which was obtained by using the statistical approximation [22]. The relative linear momentum transfer $p_{\parallel}/p_{CN}$, where p_{CN} is the momentum of a hypothetical compound nucleus formed in a complete fusion, is the main feature, considered usually as the sign of a complete fusion.

Regarding irradiations of ^{232}Th target with protons, deuterons and alpha particles on energies from 70 MeV to 1000 MeV, the information about the effect of the forward momentum ($p_{\parallel}$) imparted to the fissioning nuclei, as a function of the incident energy (E), was obtained [18]. The authors described the reaction mechanism at different energies leading to fission as:

i) low-energy range $E/A \leq 10$ MeV/u and $p_{\parallel}/p_{CN} \sim 1$. Complete fusion is the dominating process for different ions up to projectiles like ^{16}O and ^{20}Ne.

ii) energy range 10 MeV/u $\leq E/A \leq$ 70 MeV/u, $p_{\parallel}/p_{CN}$ decreases progressively down to 0.5, more than half of the incident beam momentum is transferred to the target. At such energies, different incident particles exhibit a scaling, i.e., the transferred momentum is proportional to the mass of the projectile.

iii) energy region 70 MeV/u $\leq$ E 1000 MeV/u corresponds to a transition region where the projectiles, whatever their masses, tend to transfer the same momentum. The data points indicate, being under the full momentum transfer location, the system lacks complete fusion processes.

The value of the average linear momentum transferred to the target, which was obtained in the present study, is 0.46±0.09; this quantity divided by the mass number of the projectile is plotted in Fig. 3 versus the incident energy per nucleon. The solid line represents the full momentum transfer for different projectiles and targets. The crosses denote data from this work. Our data are in good agreement with those from [18] and support the suggestion in ii), that in the energy range between 10 MeV/u and 70 MeV/u, $p_{\parallel}/p_{CN}$ decreases up to 0.5, but remains approximately independent of the target mass and of the projectile identity. Our data can confirm that a complete fusion is not the dominant process at the energy regarded.

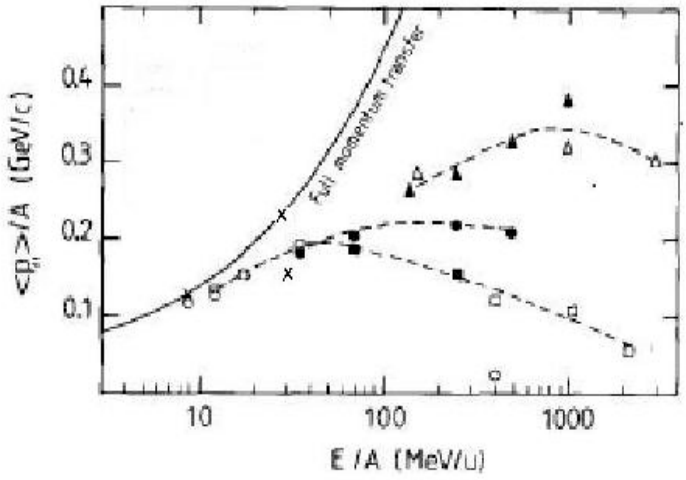

Fig. 3. Average momentum transfer per nucleon versus incident energy per nucleon [18]. The solid line is for the full momentum transfer. The dashed lines are to guide the eye. Presented symbols are for data: p + U (△), α + U (□), ^{20}Ne + U (○), p + Th (▲), d + Th (●), α + Th (■), this work (×).

Estimation of the mean excitation energies (Table 4) consists of $E^* = 90.2 \pm 18$ MeV and nuclear temperature $T = 1.9 \pm 0.2$ MeV. Both are related by the expression $aT^2 + 4T = E^*$ [23], where the parameter a is the level-density parameter equal to ($a = A/8$). For the reaction ^{208}Pb+^{6}Li at energy 94.4 MeV [5], the authors have obtained the

similar value for the excitation energy, equal to 100 MeV ($T = 2.1$ MeV), in assumption of compound nucleus channel formation. In comparison to the present work data it can be realized that with increasing projectile energy the contribution of the fusion process is reduced. That conclusion does not contradict the proposition asserted by authors in [18].

The fission cross-section in this work was found to be 604.74±90.71. The ratio between the fission cross-section σ_f and the fission cross-section for the proton-induced fission at the same excitation energy [1], is ∼5-6. Such fission cross-section increment can be associated with effect of the high transferred angular momentum during the fission process,induced by the accelerated heavy ions. As it was shown in different models [6-10] concerning macroscopic and microscopic features of the hot nuclei, the rotational energy affects the possibility of fission events. According to the dynamic model [8], heavy-ion induced fission reactions are characterized by the formation of a complete equilibrated compound nucleus. The initial relative kinetic energy and angular momentum of the projectile is converted into the intrinsic excitation energy and the spin of the fused system. It is determined by the balance among the macroscopic surface energy, the Coulomb energy, and the rotational energy contributions as well. The concept of dynamical force equilibrium in the entrance reaction channel serves as a criterion for the determination of the average and the maximum angular momentum transferred for different colliding systems. According to the model, the transferred linear momentum should be a decreasing function of the impact parameter b. Furthermore, the value of a maximum angular momentum ℓ_{max} corresponds to a peripheral collision defined by:

$$\ell_{max} = R\sqrt{\frac{2\mu(E_{c.m.} - V_{CB})}{\hbar^2}}. \tag{8}$$

Here, R is the maximum distance between two nuclei at which the collision leads to a reaction, μ is the reduced mass and V_{CB} is the Coulomb energy of the system at distance R; $E_{c.m.}$ is at the center-of-mass bombarding energy.

For the system Pb+Li at $E_{c.m.} = 237$ MeV in this work, we deduced $\ell_{max} \sim 90\,\hbar$. We estimated also the average angular momentum imparted into the fissile system. At energies above the barrier, the formula for calculation for the average angular momentum, $< \ell >$ is provided by [9]

$$< \ell >= \frac{2}{3}\sqrt{\frac{2\mu R^2(E_{c.m.} - V_{CB})}{\hbar^2}}. \tag{9}$$

The value of $< \ell >$ calculated by (9) was $< \ell >$ = 50-55 $\hbar$. For comparison, in ^{208}Pb+^{6}Li system up to energy of 94.4 MeV the angular momentum was found to be equal 30-35 $\hbar$, corresponding to a complete fusion cross-section [5]. As the projectile energy increases, the neutron evaporation also increases, opening new fission channels. As a result, there is a set of various fissioning nuclides with broad distribution of transferred linear momentum and excitation energy (eq. (7), Table 4). In [5] the angular momentum is lower, and therefore the entire linear momentum is transferred to the compound nucleus. In the data here presented, fragments are formed, from fissioning nuclei with high and low linear momentum as well. It is in complete conformity to the proposition of incomplete-fusion mechanism, in such range of energy.

The fission-barrier heights, which are function of the angular momentum, were calculated [6-10]. These heights were shown to be lower, when the angular momentum increases from the zero value. It can be realized that fission is expected to play a significant role above 50 $\hbar$, when the fission barrier has dropped to about half of the previous value, at zero angular momentum. The fission barrier decreasing can be considered, in order to analyze the energy dependence of the excited fissioning nucleus fissility [24]. The fission-barrier dependence on the angular momentum can be neglected, in the case of nucleon-nucleus interaction at intermediate energies. It holds in the energy region considered, since a merely small angular momentum is imparted to the nucleus by incident nucleons. On the another hand, it becomes relevant for higher values for ℓ, in heavy-ion-induced reactions. It provides a careful and cogent explanation for the high fission cross-section in the present investigation.

V. CONCLUSION

New data regarding the fission process in ^{7}Li+^{nat}Pb interaction were presented at intermediate energies 245 MeV. The fission cross- section, calculated on the base of charge and mass analysis was equal to 604.74±90.71. This value exceeds the cross section obtained in proton nuclear reactions at approximately the same energy range. This difference can be explained by the effect of the transferred angular momentum essentially exceeding in the ion-induced reaction.

The measurements of the recoil properties about the fission fragments, and by considering them in frames of two step models, allows to calculate the recoil parameters concerning the reaction first step. The relative value of the transferred momentum $p_{\|}/p_{CN}$ (where p_{CN} is the total momentum of the hypothetic complete nucleus), containing the information on the initial reaction mechanism, equals 0.46±0.09 approximately. This value indicates that, in the

energy range investigated, the fission process does not proceed solely via the compound nucleus formation. Other mechanisms are taking participation on the first step reaction, and only 40% of all fission events are resultant of compound nucleus fission.

Regarding the dynamic model-based calculation, the fissile system is assumed to be formed at an intermediate energy with high angular momentum. Such reason is relevant for high value of fission cross-section for heavy-ion-induced fission.

Acknowledgment

G. Karapetyan is grateful to Fundação de Amparo à Pesquisa do Estado de São Paulo (FAPESP) 2011/00314-0. and to International Centre for Theoretical Physics (ICTP) under the Associate Grant Scheme.

References

1. A. V. Prokofiev, Nucl.Instrum. Methods A **463**, 557 (2001).
2. A. Mukherjee,D. J. Hinde,M. Dasgupta, *et al.*, Phys. Rev. C **75**, 044608 (2007).
3. R. N. Sagaidak, G. N. Kniajeva, I. M. Itkis, *et al.*, Phys. Rev. C **68**, 014603 (2003).
4. A.Ingemarsson, J.Nyberg, P.U.Renberg, J*et al.*, Nucl. Phys. A **676**, 3 (2000).
5. S. E. Vigdor, H. J. Karwowski, W. W. Jacobs, *et al.*, Phys. Rev. C **26**, 1035 (1982).
6. S. Cohen, F. Plasil, and W. J. Swiatecki, Ann. Phys. (N. Y.) **82**, 557 (1974).
7. A. J. Sierk, *et al.*, Phys. Rev. C **33**, 2039 (1986).
8. J. Wilczynski, Nucl. Phys. A **216**, 386 (2073).
9. O. A. Capurro, D. E. DiGregorio, S. Gil, *et al.*, Phys. Rev. C **55**, 766 (1997).
10. M. G. Mustafa, K. Kumar, Phys. Rev. C **12**, 1638 (1975).
11. N. A. Demekhina, G. S. Karapetyan, S. M. Lukyanov, *et al.*, Phys. At.Nucl. **68**, 21 (2008766 (2005).
12. R. B. Firestone, in Tables of Isotopes, 8th ed.: 1998 Update (with CD ROM), edited by S. Y. Frank Chu (CD-ROM editor) and C. M. Baglin (Wiley Interscience, New York, 1996).
13. H. Baba, J. Sanada, H. Araki, *et al.*, Nucl.Instrum. Methods A **416**, 301 (1998).
14. H. Kudo, M. Maruyama, and M. Tanikawa, *et al.*, Phys. Rev. C **57**, 178 (1998).
15. C. L. Branquihno and V. J. Robinson, J. Inorg.Nucl. Chem. **39**, 921 (1977).
16. A. C. Wahl, R. L. Ferguson, *et al.*, Phys. Rev. **126**, 776 (1962).
17. M.C. Duijvestijn, A.J. Koning, *et al.*, Phys. Rev. C **59**, 776 (1999).
18. F. Saint-Laurent, M. Conjeaud, R. Dayrasv, *et al.*, Phys. Lett. B **110**, 372 (1982).
19. L. Winsberg, Phys. Rev. C **22**, 2116(1980).
20. L. C. Northcliffe and R. E. Schilling, Nucl.Data, Sect. A **7**, 233 (1970).
21. M. Lagarde-Simonoff and G. M. Simonoff, Phys. Rev. C **20**, 1498 (1979).
22. V. E. Viola, K. Kwiatkowski, and M. Walker, Phys. Rev. C **31**, 1550 (1985).
23. J. M. Blatt and V. F. Weisskopf,TheoreticalNuclear Physics (Wiley, New York, 1952; Inostrannaya Liter- atura, Moscow, 1954).
24. S. G. Mashnik, Acta Phys. Slov. **43**, 243 (1993).